Int. J. Environ. Sci. Technol. (2017) 14:2067–2076
DOI 10.1007/s13762-017-1308-0

ORIGINAL PAPER

Response surface methodology (RSM) optimization approach for degradation of Direct Blue 71 dye using CuO–ZnO nanocomposite

K. Salehi[1] · A. Bahmani[2] · B. Shahmoradi[1] · M. A. Pordel[1] · S. Kohzadi[1] · Y. Gong[3] · H. Guo[4] · H. P. Shivaraju[5] · R. Rezaee[1] · R. R. Pawar[6] · S.-M. Lee[6]

Received: 24 June 2016 / Revised: 14 February 2017 / Accepted: 2 March 2017 / Published online: 13 March 2017

Abstract The present study highlights the synthesis of CuO–ZnO nanocomposite via facile hydrothermal method at 150 °C and autogenous pressure. The structural and textural features of prepared composite material was characterized by several characterization techniques such as X-ray powder diffraction, Fourier transform infrared spectroscopy, Scanning electron microscopy, and energy-dispersive X-ray spectroscopy. The optimized prepared nanocomposite was utilized for photocatalytic degradation of aromatic Direct Blue 71 dye (DB71) under natural sunlight conditions. The catalytic activity results by CuO–ZnO nanocomposite were observed to be higher than the reagent-grade zinc oxide under visible light conditions. The response surface methodology protocol (RSM) with central composite design was optimized by different photodegradation operational parameters such as pH, dye concentration, catalyst amount, and reaction time. The optimized RSM results demonstrated that a quadratic polynomial model was found suitable to define the relation between the photocatalytic activity and operational parameters. Moreover, the observed high R^2 value (0.9786) confirms a strong evaluation of experimental data. To achieve maximum DB71 degradation, optimized condition was found at 177.13 min of contact time, 3.93 solution pH, and 24.34 mg/L of dye concentration with 1.85 g/L of catalyst dose The identical optimum conditions resulted maximum 89.58% DB71 degradation.

Keywords CuO–ZnO · Degradation · Modeling · Optimization · Photocatalysis · Nanocomposite

Editorial responsibility: Agnieszka Galuszka.

Electronic supplementary material The online version of this article (doi:10.1007/s13762-017-1308-0) contains supplementary material, which is available to authorized users.

✉ S.-M. Lee
leesm@cku.ac.kr

[1] Environmental Health Research Center, Kurdistan University of Medical Sciences, Sanandaj, Iran

[2] Department of Health Education, Shahid Sadoughi University of Medical Sciences and Health Services, Yazd, Iran

[3] Kazuo Inamori School of Engineering, Alfred University, Alfred, NY 14802, USA

[4] School of Materials Science and Engineering, Shaanxi University of Science and Technology, Xi'an 712000, Shaanxi, People's Republic of China

[5] Department of Life Science, School of Life Science, J.S.S. University, Shivarathreeshwara Nagara, Mysore 570015, India

[6] Department of Energy and Environment Convergence Technology, Catholic Kwandong University, 522 Naegok-dong, Gangneung 210-701, Korea

Introduction

Pigments and dyes are widely used in various industries and have become an important part of daily life (Coruh and Elevli 2014; Ertugay and Acar 2014; Bhatt et al. 2012; Tunc et al. 2012). Among the various types of the dye, the azo dyes are large class of synthetic organic dyes used in various industries. It has been estimated that azo dye accounts for approximately 60–70% use in food and textile industries (Tunc et al. 2012; Salehi et al. 2016). The effluent with azo dyes into the aqueous systems is of severe concern due to its hazardous effects on human activities and for aquatic ecosystems (Puvaneswari et al. 2006; Sawant and Cho 2016). Hence, it is important to treat azo dye wastewater before discharge into the aquatic bodies or environment. There are several traditional methods already

in use to remove organic synthetic dyes from wastewaters, such as physical (Asgher and Bhatti 2012; Nasuha et al. 2010), biological (Jamal et al. 2012), electrochemical (Ghalwa et al. 2012), and chemical processes (Hua et al. 2013). However, these all techniques have some advantages and limitations. The advanced oxidation treatment processes (AOPs) have received a great attention since they are able to deal with various types of dye pollutants and many other organics in wastewater (Anouzla et al. 2009). ZnO is a well-known material utilized in the degradation of organic pollutants in aqueous system (Parsa et al. 2014; Anouzla et al. 2009). It is widely used due to the property of narrow band gap ($\sim$3.37 eV), non-toxicity, low cost of manufacturing, and high initial rate of photocatalysis (Parsa et al. 2014). However, it is observed active under ultraviolet spectrum, which limits its potential application in environmental remediation (Li et al. 2013a). Thus, it is crucial to tailor the structure and morphology of ZnO through suitable strategies in order to alter its bulk surface properties. A suitable material as an additive or dopant has been reported as a feasible way to tailor the photocatalytic performance of ZnO under visible spectrum (Shahmoradi et al. 2010). Copper (II) oxide is a p-type semiconductor used to improve the photocatalytic efficiencies of wide band gap semiconductors such as TiO_2, ZnO, and SnO_2 (Huang et al. 2013, Mageshwari et al. 2015). The CuO–ZnO-mixed metal oxide nanoparticles are more efficient than the pure ZnO, and this is because there is condensed recombination of generated electron–hole pairs in the coupled system (Witoon et al. 2013). Coupling between two semiconductors with suitable band locations, such as ZnO and CuO, can extend the ZnO photoapproachable range to visible light and shift the photocatalytic procedure to the solar light range; (Saravanan et al. 2013; Gajendiran and Rajendran 2014). There are many reports on the synthesis of ZnO–CuO nanoparticles such as co-precipitation (Gajendiran and Rajendran 2014), thermal decomposition (Saravanan et al. 2013), sol–gel (Habibi and Rahmati 2015), hydrothermal (Li et al. 2013b), and photodeposition methods (Wang et al. 2011). Among all these methods, visible light-induced hydrothermal growth technique for synthesis of nanostructures composite is a promising and well-known synthesis method due to its characteristics including mild temperature synthesis, accurate control of composition, and controllable particle size (Maleki and Shahmoradi 2012). The hydrothermal process has several advantages over other synthesis methods including better nucleation control, simple equipment, catalyst-free growth, one-step synthesis without high-temperature calcination, and milling. In addition, the synthesized material showed a low level of aggregation and ability to obtain amorphous phase, less hazardous by-products, no need for post-treatment (Zazouli et al. 2015; Moghaddam et al. 2011).

Traditional approaches for evaluating photodegradation process are dependent on the change of one independent variable parameter such as dosage of catalyst, pH of solution, concentration of dye, while keeping all other variables constant (Shojaeimehr et al. 2014; Zazouli et al. 2015). Thus, traditional approaches resulted in additional consumption of chemicals for evaluating each parameter and eventually increased time and cost of study (Zazouli et al. 2015; Shojaeimehr et al. 2014; Moghaddam et al. 2011). In attempt to solve this issue, statistical programs such as RSM have been utilized to design of experiments and parameters optimization of process control. (Ramakrishna and Susmita 2012). The main functionality of RSM is to build the relations between numerous independent variables and responses (Danbaba et al. 2015).

RSM has been effectively utilized in various fields such as adsorption, Fenton's oxidation, electro-coagulation, and photocatalytic decolonization (Bhaumik et al. 2013; Bhatti et al. 2011; Witek-Krowiak et al. 2014; Khataee et al. 2010; Wu et al. 2012; Khataee et al. 2011). The present study investigates the effectiveness of modeling of RSM and to optimize the influencing factors on DB71 degradation using RSM approach.

Materials and methods

Materials

CuO–ZnO, trimethylamine, and NaOH were purchased from Merck, Germany. Direct Blue 71 dye was bought from AlvanSabet Co., Iran. After dilution, the specific concentration was used as a model pollutant from textile industry. Table S1 (Supplementary data) shows the chemical structure and some characteristics properties of Direct Blue 71.

Experimental methods

CuO–ZnO nanocomposites were synthesized under a mild hydrothermal condition (temperature = 150 °C, pressure = autogenous, time = 12 h). ZnO of three different concentrations (1, 2, and 3 mol), by keeping 1 mol of CuO and 10 ml of 1 mol NaOH, was added into a Teflon reactor (V_{fill} = 10 ml). A fixed concentration (1 mL) of trimethylamine was added to the above mentioned mixture, and the mixture was stirred vigorously for a few minutes. The Teflon reactor was then fixed into an autoclave. Then autoclave was sealed and reacted in an oven at 150 °C for 12 h. After 12 h of reaction, the autoclave reactor was kept at room temperature to air-quenched. The as-synthesized nanocomposite from the Teflon reactor was moved to a pre-cleaned beaker for several time washing with distilled

water and then allowed to settle down. After filtration the residue was dried at room temperature and stored prior to further use.

Photocatalytic degradation of DB71

The dye degradation efficiencies of the as-synthesized composites materials were evaluated by the photocatalytic degradation of DB71 under visible light. The tests were performed by reacting different amounts of CuO–ZnO composite (0.5–2.5 g/L) in 200 ml of the DB71 solution (20–60 mg/L) at various pH levels (3–11). The initial pH of dye solution was adjusted using a pH meter with addition of 0.1 N NaOH or HCl. Prior to exposure to natural sunlight, the DB71 solution was stirred for 30 min in dark to achieve the equilibrium between the composite and dye molecules. Subsequently, the solution with CuO–ZnO nanocomposites was illuminated under sunlight. At each scheduled time intervals, 5-ml dye solution sample was taken out from the reactor. Then, each solution sample was centrifuged for 10 min at 5000 rpm. Then the separated solutions were analyzed by UV–Vis spectrophotometer at 687 nm. The degradation efficiency removal ($R\%$) of the CuO–ZnO nanocomposite on the photodegradation of DB71 dye was calculated using Eq. 1.

$$\text{Degradation efficiency } (R\%) = (A_0 - A)/A_0 \times 100 \quad (1)$$

where A_0 is the initial concentration (mg/L) of dye and A is the concentration of dye at time t (Salehi et al. 2014).

Experimental design and data analysis

The central composite design (CCD)-based response surface methodology (RSM) is widely accepted for investigational design, modeling, and optimization. In this study, CCD statistical software design expert version 7 was used to optimize the several operational parameters for the degradation of DB71 by CuO–ZnO composite under natural sunlight. The total 31 runs were considered at 5 levels containing of 16 factorial points, 8 axial points ($\alpha = 2$), and seven replications at the center point (Table 1). The experiments were conducted in a random. The degradation percentage of DB71 as dependent variable, and other variable such as dosage of catalyst, pH of solution, contact time, and concentration of dye were chosen as independent variables in experiments.

After completion of design of experiment, the photodegradation experiments of DB71 dye were carried out to obtain an appropriate model. The obtained data were examined by quadratic models. The general form of the quadratic models is shown as follow (Eq. 2):

$$\eta = b_0 + \sum_{i=1}^{n} b_i x_i + \sum_{i=1}^{n} b_{ii} x_i^2 + \sum_{i=1}^{n-1} \sum_{i=1}^{n} b_{ij} x_i x_j \quad (2)$$

where η is the predicted response variable, b_0 is the coefficient constant, b_i is the linear coefficient, b_{ii} is the quadratic coefficient, b_{ij} is the interaction coefficient, and x_i and x_j are the coded values of the parameters (Salehi et al. 2014).

Results and discussion

Characterization of CuO–ZnO nanocomposite

The structural and textural properties of CuO–ZnO nanocomposite were investigated by various characterization techniques. Figure 1a represents the X-ray diffraction pattern of CuO–ZnO nanocomposite. A series of (100), (002), (101), and (102) reflections at $2\theta = 31.8$, 34.5, 36.3, and 47.61°, were observed in the ZnO sample, which is identical with arrangement with the wurtzite structure (JCPDS file no. 36–1451). In addition, the peaks at 2θ value of 35.5° and 38.7° belong to the CuO peaks could be easily noticed on the XRD. Peaks appears in the pattern confirms the presence of patterns of ZnO and CuO both materials in nanocomposite with and changed lattice of ZnO. The average particle size of CuO–ZnO was calculated by the Scherer formula (Eq. 3). The average size was calculated as 36 nm.

$$D_{\text{Scherrer}} = \frac{k\lambda}{\beta \cos\theta} \quad (3)$$

where D represents the average crystallite size, λ for the radiation wavelength (1.5418 Å), k is related to the crystallite shape ($k = 0.089$), β is the peak width at half maximum, and θ is the Bragg diffraction angle.

Table 1 Experimental range and levels of independent process variables

Independent variable	Factor X_i	Range and level				
		$-\alpha$	-1	0	1	$+\alpha$
Initial pH	X_1	3	5	7	9	11
Catalyst dosage (g/L)	X_2	0.5	0.1	1	1.5	2.5
Contact time (min)	X_3	60	90	130	150	180
DB71 concentration (mg/L)	X_4	30	35	40	45	50

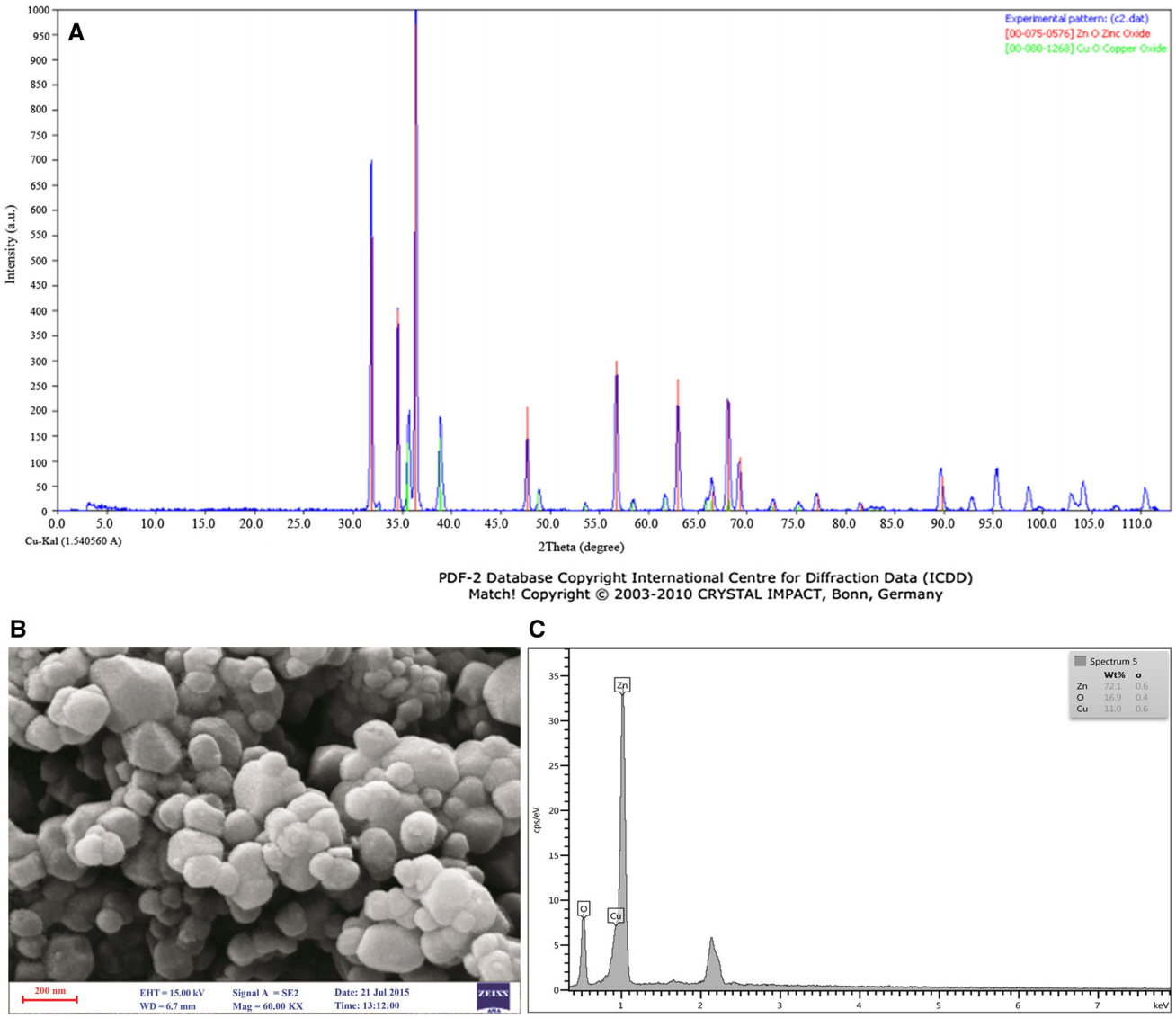

Fig. 1 **a** XRD pattern of CuO–ZnO nanocomposite, **b** SEM image, and **c** EDAX analysis of CuO–ZnO nanocomposite

The Fourier transform infrared spectroscopy (FTIR) analysis was performed to study the significance of CuO on the surface chemistry of CuO–ZnO nanocomposite and also to determine the presence of functional group impurity due to surface modifier. Figure S1 (Supplementary data) shows the FTIR profile of ZnO and CuO–ZnO nanocomposite. The spectra observed at 540 cm^{-1} represent the Zn–O, whereas the peak at 950 cm^{-1} represents the Cu–O stretching frequencies. In FTIR spectra, no new functional group peak was observed on the surface of CuO–ZnO nanocomposite indicates the whole detachment of surface modifier by several cycle of washing.

The surface morphology analysis of CuO–ZnO nanocomposite was performed by scanning electron microscopy (SEM) studies. Figure 1[B] reveals that the nanocomposites synthesized have different size and heterogeneous morphology; among them hexagonal and spherical nanocomposites are more obvious. Moreover, no aggregation was observed. Energy-dispersive spectrometry (EDAX) analysis of CuO–ZnO is suitable for confirming elemental analysis. As shown from Fig. 1c, the occurrence of the Zn, O, and Cu elements suggested the high purity of nanocomposite.

DB71 degradation studies

Effect of CuO–ZnO nanocomposite

To assess the consequence of the alteration of ZnO nanoparticles with CuO, the degradation proficiency test was carried out with reagent-grade ZnO and the synthesized CuO–ZnO nanocomposite. It was observed that the CuO–ZnO nanocomposite showed higher photocatalytic activity than reagent-grade ZnO (Fig. 2a). About 97% of

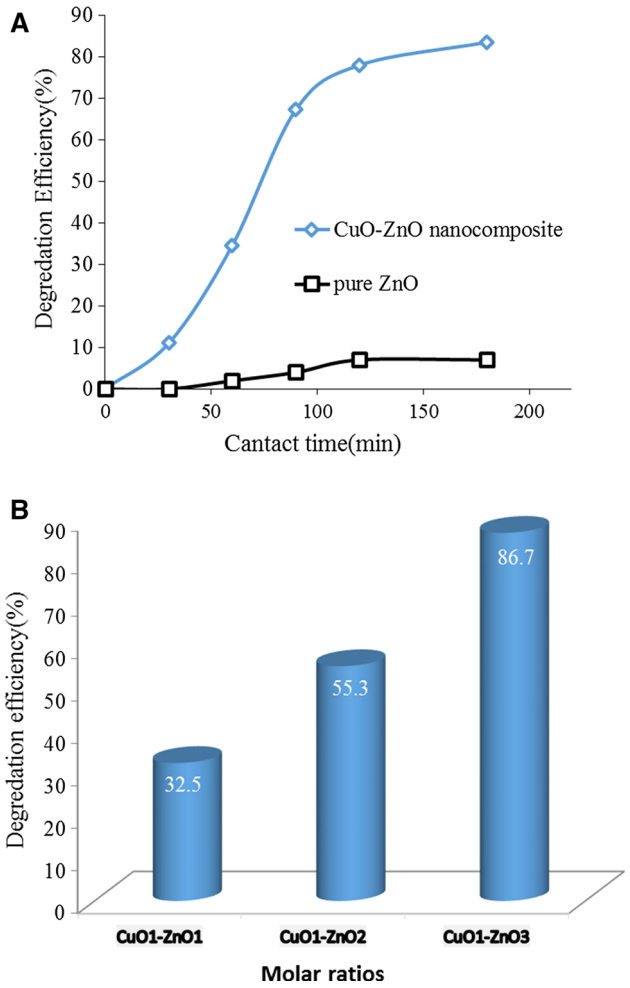

Fig. 2 **a** Comparison of degradation of DB71 in the presence of reagent-grade ZnO and CuO–ZnO nanocomposite. (DB71 concentration 20 mg/L, pH = 7, contact time = 150 min, and catalyst dosage = 1.5 g/L), **b** Effect of CuO–ZnO molar ratio in the presence of 1.5 g/L of catalyst, an initial dye concentration of 20 mg/L and PH = 5 for 25 min

the DB71 was degraded by CuO–ZnO after 180 min of exposure to natural sunlight, whereas only 7% of DB71 was degraded by reagent-grade ZnO under the identical conditions. The higher photocatalytic performance of CuO–ZnO nanocomposite can be explained by enhanced quantum efficiency of visible light absorption (Shahmoradi et al. 2012). Panneerselvam and coworkers evaluated the absorbance bands for simple ZnO and coupled semiconductor CuO–ZnO composite. The absorbance onset was at about 385 nm for unmodified ZnO particles, whereas CuO–ZnO composite displays blueshift. Additionally, a broad absorption band seen around 550–800 nm might be attributed due to the presence of Cu^{2+} species in the prepared CuO–ZnO nanocomposites (Sathishkumar et al. 2011). Hence, reagent-grade ZnO was not included as a variable for further photodegradation studies.

Influence of CuO–ZnO molar ratio

The catalytic activities of the samples with variable molar ratios (1:1, 1:2, and 1:3) of CuO–ZnO nanocomposites were used for the degradations of DB71, and the observed results are presented in Fig. 2b. It can be observed from the obtained results that, the sample with molar ratio 1:3 of CuO–ZnO shows the highest photocatalytic activity toward DB71 degradations. Therefore, the entire photodegradation experiments were conducted using 1:3 CuO–ZnO nanocomposite.

Modeling and optimization of DB71 degradation

The investigational results of DB71 photodegradation using as-synthesized CuO–ZnO nanocomposite were examined through response surface methodology to attain an empirical model. Based on these consequences, the association between the degradation of DB71 and the independent variables parameters was achieved and stated by the second-order polynomial equation (Eq. 4):

$$\begin{aligned} R = {} & (-35.97) + (3.668X_1) + (63.023X_2) + (0.6833X_3) \\ & + (0.91328X_4) + (-0.5906X_1X_2) + (-0.01005X_1X_3) \\ & + (0.023X_1X_4) + (0.0693X_2X_3) + (+0.0218X_1X_4) \\ & + \left(-0.2594X_1^2\right) + \left(-15.86X_2^2\right) + \left(-1.1429X_3^2\right) \\ & + \left(-0.022304X_4^2\right) \end{aligned} \quad (4)$$

where R is response degradation percent, X_1, X_2, X_3, and X_4 are the corresponding independent parameters such as pH, catalyst amount (g/l), reaction time (min), and DB71 initial concentration (mg/L), respectively.

Table 2 shows the outcomes of ANOVA study of the quadratic models. The significance of each coefficient was calculated by the F test and p value. The values of Prob > F less than 0.05 and more than 0.1000 indicate the model terms are not significant and significant, respectively. In Table 3, the terms are significant for X_1, X_2, and X_3, but those are not significant for X_1X_2, X_2X_3, X_2X_4, X_3X_4 according to Prob > F values. The "lack of fit F value" 0.2600 for the model obtained implies the deficiency of fit insignificancy, and the model is adequate. Acceptable precision is calculated for the signal-to-noise ratio, and a ratio larger than 4 is generally essential. In this research, precision obtained was 24.78 for the degradation percentage of DB71. The ratio determined was greater than 4, and the representative for the model can be used to navigate the design space (Moghaddam et al. 2011).

Moreover, ANOVA indicated that the coefficient of determination (R^2) and adjusted R^2 were 0.9786 and 0.9585, respectively. The values of coefficient of determination and the adjusted R^2 are succeeded to estimate the

Table 2 ANOVA of the quadratic model of photo catalyst degradation of DB71 dye using CuO–ZnO nanocomposite

Source	Sum of square	*df*	Mean square	*f* value	*p* value
Model	6989.36	14	499.28	48.90	<0.0001 sign
X_1	2682.88	1	2682.88	262.78	<0.0001
X_2	375.90	1	375.90	36.82	<0.0001
X_3	283.48	1	283.48	27.77	<0.0001
X_4	37.24	1	37.24	3.65	0.0755
X_1X_2	1.93	1	1.93	0.19	0.6703
X_1X_3	38.91	1	38.91	3.81	0.0698
X_1X_4	3.20	1	3.20	0.31	0.5831
X_2X_3	1.72	1	1.72	0.17	0.6870
X_2X_4	5.58	1	5.58	0.55	0.4711
X_3X_4	5.82	1	5.82	0.57	0.4919
X_1^2	136.23	1	136.23	13.34	0.0024
X_2^2	431.46	1	431.46	42.26	<0.0001
X_3^2	29.02	1	29.02	2.84	0.1124
X_4^2	28.32	1	28.32	2.77	0.1165
Residual	153.14	15	10.21	–	–
Lack of fit	120.41	10	12.04	1.84	0.2600 not sign
Total	12,504	30	–	–	–

Table 3 Optimum values of the process parameter for maximum efficiency

Parameter	DB71 Optimum values
η (efficiency, %)	89.58
X_1 (pH)	3.93
X_2 (catalyst dosage)	1.85
X_3 (contact time, g/L)	177.13
X_4 (concentration dye, mg/L)	24.34

fitting of the model. The obtained R^2 in DB71 degradation using CuO–ZnO nanocomposite indicated a stronger association between the factors and predicted results.

Figure 3 represents the connection between experimental and projected value for degradation of DB71 using CuO–ZnO composite. The obtained results showed that the experimental and predicted values for dye degradation were found higher, and the present model well fits the experimental data. Therefore, the model could be used to calculate the dye degradation in the investigational range of variables.

Figure 4 represents the plots of residuals against normal probability for DB71 degradation. As shown in plot, obtained data show a linear relationship, which indicates distributed normal distribution of residuals. Thus, it is concluded that the prediction of the experimental results obtained from the developed quadratic model is satisfactory in the parameterization of the degradation of DB71.

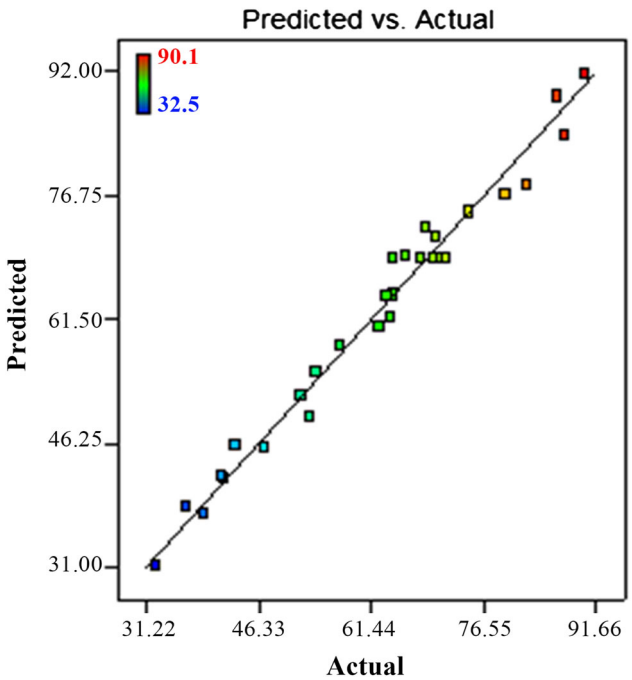

Fig. 3 A plot of the predicted versus the experimental degradation efficiency

Response surface plotting for estimation of operating variables

Influence of initial solution pH

The consequence of the pH on the DB71 degradation efficacy results is shown in Fig. 5, at a composite dosage of

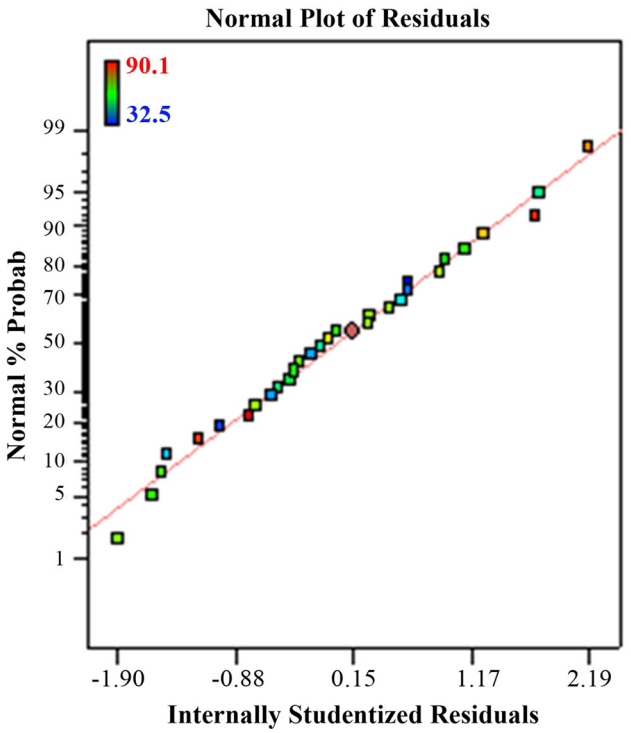

Fig. 4 A plot of the normal probability of the raw residuals

1.5 g/L and early dye concentration ~20 mg/L. As shown in plot, the degradation efficiency (%) of DB71 increases from pH 3–7 and then reduces at the higher pH 11. The increase in pH from 3.0 to 7.0 resulted in an increase in DB71 degradation efficiency from 46.8 to 70.2%, and the efficiency decreases from 70.2 to 62% as the pH increases from 7 to 11. Such phenomenon may be observed due to the change in electrostatic magnetism or revulsion among DB71 molecules and the nanocomposite. The surface charge of nanocomposite has a significant effect on the adsorption and dissociation of DB71. The pH_{pZC} (point of zero charge) of ZnO was already reported as 9 ± 0.3 (Shibin et al. 2014), which suggests that the nanocomposite surface must be positively charged at the pH of 3–7 and negative at the pH of 7–11. Given the fact that DB71 is an anionic dye, it has a high efficiency to be adsorbed onto the nanocomposite surface when the pH is $<pH_{ZPC}$. Therefore, the degradation efficiency of DB71 increases accordingly when pH is $<pH_{ZPC}$ (Mohaghegh et al. 2014; Nilamadanthai et al. 2013).

Influence of catalyst amount

Figure 6 shows the influence of nanocomposite amount on the degradation efficiency of DB71 concentration of 20 mg/L and a contact time of 150 min. As shown in profile the degradation productivity increases as the CuO–ZnO dosage increases from 0.50 to 2.0 g/L and then decreases as the dosage increases from 2 g/L to the maximum value of 2.5 g/L. These results showed that the increase in composite dosage improved the degradation efficiency of the dye by increasing the number of active sites for the catalytic events. Moreover, the degradation efficacy of the dye decreases due to the interruption of light by the aqueous suspension and agglomeration in nanocomposite when the loading of nanocomposite exceeds the limiting value (2 g/L). Additionally, at a higher level of catalyst dosage, the aggregation of catalyst causes a reduction in the active surface sites and increases the scattering of light, which eventually lead to the inhibition of the photon absorption of CuO–ZnO nanocomposite (Senthilraja et al. 2014; Harraz et al. 2014).

Influence of the dye concentration

The consequence of initial dye concentration on the photodegradation efficacy is shown in Fig. 7 at a contact time of 150 min and an initial pH of 8. The effect of concentration plot showed that the degradation efficiency decreased from 73 to 22% by enhancing the initial dye concentration from 20 to 60 mg/L. This was observed due to the presence of hydroxyl radical (OH) on the composite surface and the probability of hydroxyl radicals interacting with the dye molecule. Additionally, the decrease in degradation efficiency at higher dye concentration could be due to the reduction in the path length of photons entering the solution when the solution was intensively colored at higher dye concentration. Thus, fewer photons reached the nanocomposite surface (Harraz et al. 2014; Kaur et al. 2013).

Process optimization

It is important to control the optimized circumstances of photodegradation in direction to enhance the degradation efficacy using developed mathematical model. Hence, the experimental variable parameters were set to the values in the considered range, while the response was set to a maximum level. In this approach, the optimal conditions for dye degradation using CuO–ZnO nanocomposite were determined to be contact time of 177.13 min, initial solution pH of 3.93, dye concentration of 24.34 mg/L, and a dosage of catalyst of 1.85 g/L. Under these conditions, a high degradation efficiency of 89.58% was achieved (Table 3).

Conclusion

In this research, the synthesis, characterization, modeling, and optimization of CuO–ZnO nanocomposite for the degradation DB71 was investigated. The prepared CuO–

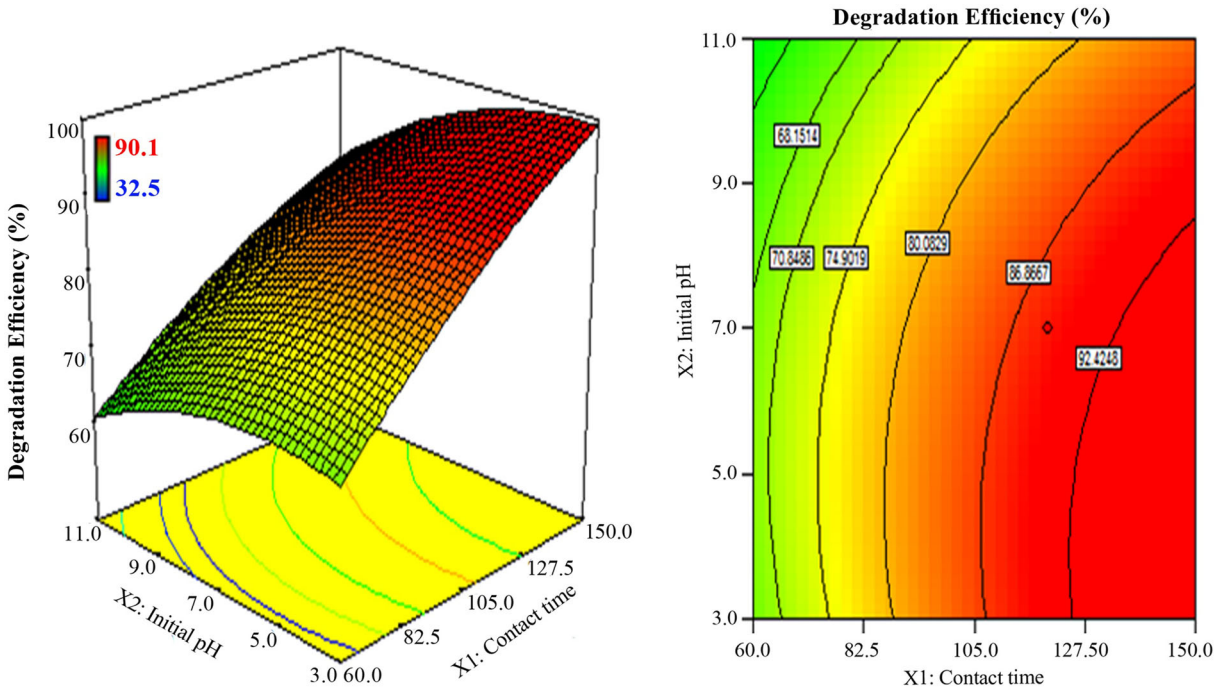

Fig. 5 Response surface plot and counter plot of the DB71 as a function of initial pH and reaction time (CuO–ZnO = 1.5 g/L, initial dye concentration = 20 mg/L)

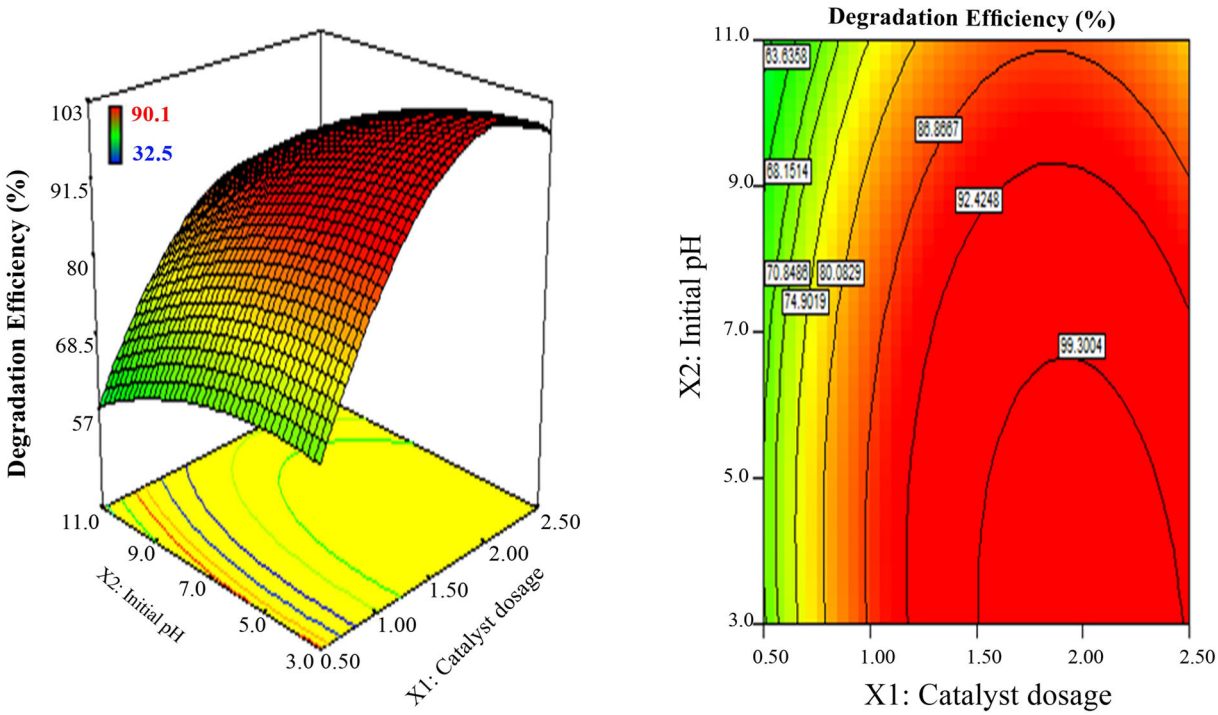

Fig. 6 Response surface plot and counter plot of the DB71 as a function of initial catalyst dosage (g/L) and Initial pH, contact time = 150 min, initial dye concentration = 20 mg/L

ZnO nanocomposite was characterized using XRD, FTIR, SEM, and EDS. The CCD was effectively applied for the design of experiment and analysis of results. The obtained correlation coefficient R^2 was found 0.9786 for DB71, indicating that the experimental data fit well with the modeling data obtained from the as-developed quadratic

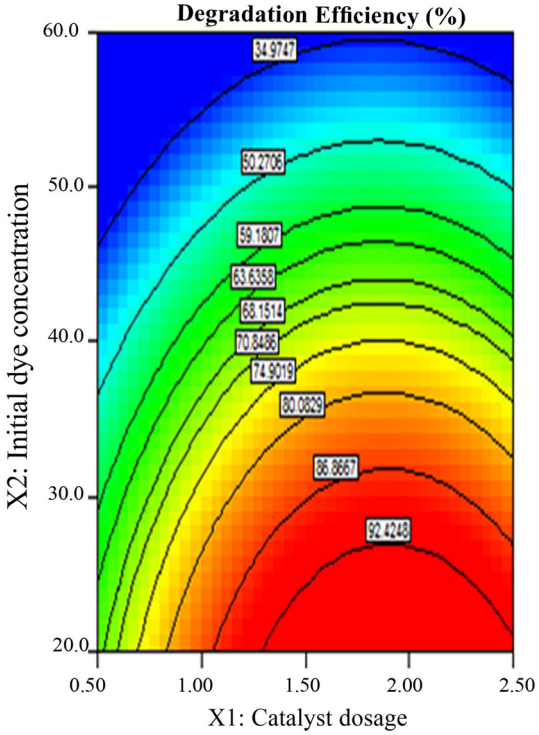

Fig. 7 Response surface plot and counter plot of the DB71 degradation as a function of initial dye concentration and initial catalyst dosage, pH = 7, reaction time = 150 min

models. The influence of solution pH, dosage of catalyst, contact time, and dye concentration at optimal experimental conditions was evaluated. The optimum photodegradation efficiency (89.58%) was found at an initial pH of 3.93, dosage of catalyst of 1.85 g/L, dye concentration of 20.34 mg/L, and reaction time of 177.13 min. The investigational values were found promising with the predicted values from the developed quadratic model. This study sheds light on the potential applications of response surface methodology in the modeling and optimization of photodegradation of aromatic dyes.

Acknowledgements The authors are thankful to Prof. A. Maleki of Kurdistan University of Medical Sciences, Sanandaj, Iran, for funding sources and the laboratory facilities.

References

Anouzla A, Abrouki Y, Souabi S, Safi M, Rhbal H (2009) Colour and COD removal of disperse dye solution by a novel coagulant: application of statistical design for the optimization and regression analysis. J Hazard Mater 166:1302–1306

Asgher M, Bhatti HN (2012) Removal of reactive blue 19 and reactive blue 49 textile dyes by citrus waste biomass from aqueous solution: equilibrium and kinetic study. Can J Chem Eng 90:412–419

Bhatt AS, Sakaria PL, Vasudevan M, Pawar RR, Sudheesh N, Bajaj HC, Mody HM (2012) Adsorption of an anionic dye from aqueous medium by organoclays: equilibrium modeling, kinetic and thermodynamic exploration. RSC Adv 2:8663–8671

Bhatti MS, Reddy AS, Kalia RK, Thukral AK (2011) Modeling and optimization of voltage and treatment time for electrocoagulation removal of hexavalent chromium. Desalination 269:157–162

Bhaumik R, Mondal NK, Chattoraj S, Datta JK (2013) Application of response surface methodology for optimization of fluoride removal mechanism by newely developed biomaterial. Am J Anal Chem 4:404

Coruh S, Elevli S (2014) Optimization of malachite green dye removal by sepiolite clay using a central composite design. Global NEST J 16:339–347

Danbaba N, Nkama I, Badau MH (2015) Application of response surface methodology (RSM) and central composite design (CCD) to optimize minerals composition of rice-cowpea composite blends during extrusion cooking. Int J Food Sci Nutr Eng 5:40–52

Ertugay N, Acar FN (2014) The degradation of Direct Blue 71 by sono, photo and sonophotocatalytic oxidation in the presence of ZnO nanocatalyst. Appl Surf Sci 318:121–126

Gajendiran J, Rajendran V (2014) Synthesis and characterization of coupled semiconductor metal oxide (ZnO/CuO) nanocomposite. Mater Lett 116:311–313

Ghalwa NA, Gaber M, Khedr AM, Salem MF (2012) Comparative study of commercial oxide electrodes performance in electrochemical degradation of reactive orange 7 dye in aqueous solutions. Int J Electrochem Sci 7:6044–6058

Habibi MH, Rahmati MH (2015) The effect of operational parameters on the photocatalytic degradation of Congo red organic dye using ZnO–CdS core–shell nano-structure coated on glass by Doctor Blade method. Spectrochim Acta Part A Mol Biomol Spectrosc 137:160–164

Harraz F, Mohamed R, Rashad M, Wang Y, Sigmund W (2014) Magnetic nanocomposite based on titania–silica/cobalt ferrite for photocatalytic degradation of methylene blue dye. Ceram Int 40:375–384

Hua L, Ma H, Zhang L (2013) Degradation process analysis of the azo dyes by catalytic wet air oxidation with catalyst CuO/γ-Al_2O_3. Chemosphere 90:143–149

Huang J, Dai Y, Gu C, Sun Y, Liu J (2013) Preparation of porous flower-like CuO/ZnO nanostructures and analysis of their gas-sensing property. J Alloys Compd 575:115–122

Jamal F, Singh S, Qidwai T, Pandey PK, Singh D (2012) Optimization of internal conditions for biocatalytic dye color removal and a comparison of redox mediator's efficiency on partially purified Trichosanthes dioica peroxidase. J Mol Catal B Enzym 74:116–124

Kaur J, Bansal S, Singhal S (2013) Photocatalytic degradation of methyl orange using ZnO nanopowders synthesized via thermal decomposition of oxalate precursor method. Phys B 416:33–38

Khataee AR, Zarei M, Moradkhannejhad L (2010) Application of response surface methodology for optimization of azo dye removal by oxalate catalyzed photoelectro-Fenton process using carbon nanotube-PTFE cathode. Desalination 258:112–119

Khataee A, Kasiri M, Alidokht L (2011) Application of response surface methodology in the optimization of photocatalytic removal of environmental pollutants using nanocatalysts. Environ Technol 32:1669–1684

Li C, Hu R, Qin L, Ding R, Li X, Wu H (2013a) Enhanced photocatalytic activity of ZnO/La_2O_3 composite modified by potassium for phenol degradation. Mater Lett 113:190–194

Li Z, Zhou Z, Yun G, Shi K, Lv X, Yang B (2013b) High-performance solid-state supercapacitors based on graphene-ZnO hybrid nanocomposites. Nanoscale Res Lett 8:1–9

Mageshwari K, Nataraj D, Pal T, Sathyamoorthy R, Park J (2015) Improved photocatalytic activity of ZnO coupled CuO nanocomposites synthesized by reflux condensation method. J Alloys Compd 625:362–370

Maleki A, Shahmoradi B (2012) Solar degradation of Direct Blue 71 using surface modified iron doped ZnO hybrid nanomaterials. Water Sci Technol 65:1923–1928

Moghaddam SS, Moghaddam MA, Arami M (2011) qResponse surface optimization of acid red 119 dye from simulated wastewater using Al based waterworks sludge and polyaluminium chloride as coagulant. J Environ Manag 92:1284–1291

Mohaghegh N, Tasviri M, Rahimi E, Gholami MR (2014) Nano sized ZnO composites: preparation, characterization and application as photocatalysts for degradation of AB92 azo dye. Mater Sci Semicond Process 21:167–179

Nasuha N, Hameed B, Din ATM (2010) Rejected tea as a potential low-cost adsorbent for the removal of methylene blue. J Hazard Mater 175:126–132

Nilamadanthai A, Sobana N, Subash B, Swaminathan M, Shanthi M (2013) Photocatalytic destruction of an organic dye, Acid Red 73 in aqueous ZnO suspension using UV light energy. Indian J Chem 52:63–67

Parsa JB, Golmirzaei M, Abbasi M (2014) Degradation of azo dye CI Acid Red 18 in aqueous solution by ozone-electrolysis process. J Ind Eng Chem 20:689–694

Puvaneswari N, Muthukrishnan J, Gunasekaran P (2006) Toxicity assessment and microbial degradation of azo dyes. Indian J Exp Biol 44:618

Ramakrishna G, Susmita M (2012) Application of response surface methodology for optimization of Cr(III) and Cr(VI) adsorption on commercial activated carbons. Res J Chem Sci. ISSN: 2231-606X

Salehi K, Daraei H, Teymouri P, Maleki A (2014) Hydrothermal synthesis of surface-modified copper oxide-doped zinc oxide nanoparticles for degradation of acid black 1: modeling and optimization by response surface methodology. J Adv Environ Health Res 2:101–109

Salehi K, Shahmoradi B, Bahmani A, Pirsaheb M, Shivaraju H (2016) Optimization of reactive black 5 degradation using hydrothermally synthesized NiO/TiO2 nanocomposite under natural sunlight irradiation. Desalin Water Treat 57(52):1–11

Saravanan R, Karthikeyan S, Gupta V, Sekaran G, Narayanan V, Stephen A (2013) Enhanced photocatalytic activity of ZnO/CuO nanocomposite for the degradation of textile dye on visible light illumination. Mater Sci Eng, C 33:91–98

Sathishkumar P, Sweena R, Wu JJ, Anandan S (2011) Synthesis of CuO–ZnO nanophotocatalyst for visible light assisted degradation of a textile dye in aqueous solution. Chem Eng J 171:136–140

Sawant SY, Cho MH (2016) Facile and single-step route towards ZnO@C core-shell nanoparticles as an oxygen vacancy induced visible light active photocatalyst using the thermal decomposition of Zn(an)2(NO_3)2. RSC Adv 6:70644–70652

Senthilraja A, Subash B, Krishnakumar B, Rajamanickam D, Swaminathan M, Shanthi M (2014) Synthesis, characterization and catalytic activity of co-doped Ag–Au–ZnO for MB dye degradation under UV-A light. Mater Sci Semicond Process 22:83–91

Shahmoradi B, Ibrahim IA, Sakamoto N, Ananda S, Somashekar R, Row TNG, Byrappa K (2010) Photocatalytic treatment of municipal wastewater using modified neodymium doped TiO_2 hybrid nanoparticles. J Environ Sci Health, Part A 45:1248–1255

Shahmoradi B, Negahdary M, Maleki A (2012) Hydrothermal synthesis of surface-modified, manganese-doped TiO_2 nanoparticles for photodegradation of methylene blue. Environ Eng Sci 29:1032–1037

Shibin OM, Rajeev B, Veena V, Yesodharan EP, Yesodharan S (2014) ZnO photocatalysis using solar energy for the removal of trace amounts of alfa-methylstyrene, diquat and indigo carmine from water. J Adv Oxid Technol 17:297–304

Shojaeimehr T, Rahimpour F, Khadivi MA, Sadeghi M (2014) A modeling study by response surface methodology (RSM) and artificial neural network (ANN) on Cu 2 + adsorption optimization using light expended clay aggregate (LECA). J Ind Eng Chem 20:870–880

Tunc S, Gürkan T, Duman O (2012) On-line spectrophotometric method for the determination of optimum operation parameters on the decolorization of Acid Red 66 and Direct Blue 71 from aqueous solution by Fenton process. Chem Eng J 181:431–442

Wang J, Fan X, Wu D, Dai J, Liu H, Liu H, Zhou Z (2011) Fabrication of CuO/T-ZnOw nanocomposites using photodeposition and their photocatalytic property. Appl Surf Sci 258:1797–1805

Witek-Krowiak A, Chojnacka K, Podstawczyk D, Dawiec A, Pokomeda K (2014) Application of response surface methodology and artificial neural network methods in modelling and optimization of biosorption process. Bioresour Technol 160:150–160

Witoon T, Permsirivanich T, Chareonpanich M (2013) Chitosan-assisted combustion synthesis of CuO–ZnO nanocomposites: effect of pH and chitosan concentration. Ceram Int 39:3371–3375

Wu J, Zhang H, Oturan N, Wang Y, Chen L, Oturan MA (2012) Application of response surface methodology to the removal of the antibiotic tetracycline by electrochemical process using carbon-felt cathode and DSA (Ti/RuO 2–IrO 2) anode. Chemosphere 87:614–620

Zazouli M, Safarpour M, Dobaradaran S, Veisi F (2015) Modeling of nitrate removal from aqueous solution by fe-doped TiO_2 under UV and solar irradiation using response surface methodology. Glob NEST J 17:379–388